JOINT INSTITUTE FOR NUCLEAR RESEARCH
Flerov laboratory of Nuclear Reactions

FINAL REPORT ON THE SUMMER STUDENT PROGRAM

SHI Tracks Modelling in Polymers

Supervisor:
Dr. Ruslan Rymzhanov

Student:
Fedor Akhmetov, Russia
NRNU MEPhI

Participation period:
September 08 – November 02

Dubna, 2019

Abstract

Mermin Energy Loss Function (Mermin ELF) is one of the most popular models for description of electron kinetics of various polymers and biomolecules. We present exact form of the Mermin ELF and compare it with standard models from Monte Carlo code TREKIS, which is the powerful instrument for modelling initial excitation and relaxation of electronic subsystem in the vicinity of the Swift Heavy Ion (SHI) trajectory for various materials. We also calculate initial kinetics for polyethylene $(C_2H_4)_n$ and use it like initial condition in coarse-grained molecular dynamics simulation of the SHI track formation.

Contents

1 Introduction

Irradiation with swift heavy ions (SHI, $M \geq 20m_p, E > 1MeV / nucl$) decelerated in the electronic stopping regime has been actively interested as a possible tool for ion cancer therapy and genome editing [1]. The high amount of energy deposited into a polymer or biomolecule can break the bonds between monomers, which will lead to a change in the molecular structure of the target.

The main channel of target excitation is the excitation of the electron subsystem, resulting in generation of fast electrons. Event-by-event Monte Carlo (MC) code TREKIS [2] describes spreading of electrons and holes and their interaction with matter in the nanometric vicinity of the SHI trajectory [3].

For adequate description of initial electron kinetics within SHI track is necessary to know appropriate cross sections of an ion and electrons scattering on the system of strongly correlated electrons. Here we use the Complex Dielectric Function (CDF) formalism to construct realistic cross sections. We examine several CDF models that are most often used for description of the interaction of a charged particle with matter.

We calculate radial distributions of electrons and holes and their energy density generated in SHI tracks in polyethylene at different times up to 100 fs after passage of Pb 850 MeV ions. These data are used to molecular dynamic modelling relaxation of the ionic subsystem and further structural transformations in track.

2 Model

2.1 Complex dielectric function formalism

The cross section of a charged particle on the system of strongly correlated particles can be represented within 1st Born approximation as the product of cross section of scattering on an individual particle and the dynamic structure factor (DSF) of the electrons. According to fluctuation-dissipation theorem, DSF can be expressed in terms of the imaginary part of the inverse CDF [4], [5], [6]:

$$\frac{\partial^2\sigma}{\partial(\hbar\omega)\partial(\hbar q)} = \frac{2\left(Z_e e\right)^2}{n_{sc}\pi\hbar^2 v^2}\frac{1}{\hbar q}\left(1-e^{-\frac{\hbar\omega}{k_B T}}\right)^{-1} Im\left(\frac{-1}{\varepsilon(\omega,q)}\right) \tag{1}$$

here σ is the cross section of a scattering particle, e is the electron charge, $\hbar\omega$ is the transferred energy, v is the velocity of incident particle, Z_e is the effective charge of the particle penetrating through the (for an incident electron $Z_e = 1$, for an ion we use the Barkas formula [7]), T is the temperature of the target, n_{sc} is the density of scattering centers. $\varepsilon(\omega,q)$ is the complex dielectric function and his inverse imaginary part is called the energy loss function (ELF).

The main measured experimentally parameters of a projectile are the inelastic mean free path $\lambda = (n\sigma)^{-1}$ and the energy loss $-dE/dx$ [8].

$$\lambda^{-1} = \int_{E_{min}}^{E_{max}}\int_{q_-}^{q_+}\frac{\partial^2\lambda^{-1}}{\partial(\hbar\omega)\partial(\hbar q)}d(\hbar\omega)d(\hbar q) \tag{2}$$

$$-\frac{dE}{dx} = \int_{E_{min}}^{E_{max}}\int_{q_-}^{q_+}\frac{\partial^2\lambda^{-1}}{\partial(\hbar\omega)\partial(\hbar q)}(\hbar\omega)d(\hbar\omega)d(\hbar q) \tag{3}$$

The lower integration limit $E_{min} = E_{th}$ is threshold energy of shell (band gap for valence band and ionization potential for deep shells). The upper limit of integration is $E_{max} = \frac{4E_{in}m_e M_{in}}{(m_e + M_{in})^2}$ for ion, where E_{in} and M_{in} are energy and mass of ion. For the incident electron $E_{max} = \frac{E_{in} + E_{th}}{2}$, accounting for the identity of electrons. The limits of the integration over the momentum are $q_\pm = \sqrt{2m_e/\hbar^2}\left(\sqrt{E_{in}} \pm \sqrt{E_{in} - \hbar\omega}\right)$ for the electrons, $q_- = E_{in}/\hbar v, q_+ = \sqrt{2m_e E_{max}/\hbar^2}$ for the ions.

2.2 Ritchie algorithm for CDF fitting

The inverse imaginary part of the CDF may be reconstructed from the measured optical coefficients for valence band and x-ray attenuation lengths for deep shells as follows:

$$\left(\frac{-1}{\varepsilon(0,\omega)}\right)_{\exp} = \frac{2nk}{(n^2-k^2)^2-(2nk)^2}\theta(\omega-\omega_{gap}) + \sum_i \frac{c}{\omega\lambda_i}\theta(\omega-\omega_{i,th}) \quad (4)$$

the low energy optical constants for most common materials are available here [9] while attenuation lengths can be found in [10].

According to Ritchie and Howie, experimental ELF can be expressed in terms of sum of Drude-Lorentz oscillator functions [5]:

$$\left(\frac{-1}{\varepsilon(0,\omega)}\right)_{\exp} \approx \sum_n \frac{A_n}{E_n^2}\left(\frac{-1}{\varepsilon_D(0,\omega,\gamma_n,E_n)}\right) = \sum_n \frac{A_n}{E_n^2}\frac{E_n^2\omega\gamma_n}{((\omega^2-E_n^2)^2+(\gamma_n\omega)^2)} \quad (5)$$

here E_n means the characteristic energy of the oscillator n, A_n is the fraction of electrons with energy E_n, and γ_n is the nth energy damping coefficient; the summation is running through the all oscillators.

The quality of the fit is determined by checking whether the energy loss function satisfies the sum rules.

The first is *f*-sum rule says that the value

$$Z_{eff} = \frac{2}{\pi\omega_{pl}^2}\int_0^{\omega_{max}}\left(\frac{-1}{\varepsilon(\omega,q)}\right)\omega d\omega \quad (6)$$

must be equal to the total number of electrons per molecule of a target when $\omega_{max}\to\infty$. Here $\omega_{pl} = \frac{4\pi e^2 n_m}{m_e}$ is plasmon frequency, n_m is the density of molecules.

The second is *ps*-sum rule:

$$P_{eff} = \frac{2}{\pi}\int_0^{\omega_{max}}\left(\frac{-1}{\varepsilon(\omega,q)}\right)\frac{d\omega}{\omega} \quad (7)$$

must be equal to unity when $\omega_{max}\to\infty$.

2.3 Choice of dispersion relation

The CDF fitted from the optical data does not contain the dependence on the transferred momentum, because in the optical limit the momentum transferred to the system is equal to zero within dipole approximation. There are several methods to introduce momentum-dependence into the CDF. One of this methods is based on dispersion relations for the energy of nth oscillator $E_n = E_n(q)$.

1) The simplest approximation is free-particle approximation [5]

$$E_n(q) = E_n + \frac{\hbar^2 q^2}{2m} \quad (8)$$

where m is the mass of a scattering centre, $m = m_e$ for scattering on the electron subsystem.

2) The plasmon pole approximation is often used for electrons [11]:

$$E_n^2(q) = E_n^2 + \frac{1}{3}v_f^2(\hbar q)^2 + \left(\frac{\hbar^2 q^2}{2m_e}\right)^2 \tag{9}$$

where v_f is the Fermi velocity of electrons in the target.

3) Ritchie approximation [5]:

$$E_n(q) = \left[E_n^{2/3} + \left(\frac{\hbar^2 q^2}{2m_e}\right)^{2/3}\right]^{3/2}, \quad \gamma_n(q) = \left[\gamma_n^2 + \left(\frac{\hbar^2 q^2}{2m_e}\right)^2\right]^{1/2} \tag{10}$$

For the most materials we use free-electron approximation, because it works well at least at the limit of high energies and at the limit of zero transferred energy. For the intermediate energies (~1 eV – 100 eV) the inelastic mean free paths may be differ from the experimental data, however, for most materials studied, the calculations are in good agreement with experiment.

2.4 Mermin-type ELF

Another way to extend to arbitrary momentum is using of Mermin model for CDF [12]. Mermin model is the correction of the random-phase approximation CDF for the finite lifetime of particles. The Mermin function is expressed through a combination of t the Lindhard (RPA) dielectric functions as follows:

$$\varepsilon_M(q,\omega) = 1 + \frac{\left(1+\frac{i\gamma}{\omega}\right)\left(\varepsilon_L(q,\omega+i\gamma)-1\right)}{1+\frac{i\gamma}{\omega}\frac{\varepsilon_L(q,\omega+i\gamma)-1}{\varepsilon_L(q,0)-1}} \tag{11}$$

It is easy to calculate, that in the limit of zero momentum Mermin ELF reduces to the Drude-Lorentz ELF:

$$\mathrm{Im}\left(\frac{-1}{\varepsilon_M(0,\omega)}\right) = \mathrm{Im}\left(\frac{-1}{\varepsilon_{DL}(0,\omega)}\right) = \frac{\omega\gamma E^2}{(\omega^2 - E^2)^2 + (\omega\gamma)^2} \tag{12}$$

This allows to use sum of Mermin energy loss functions like approximation for experimental energy loss function

$$\left(\frac{-1}{\varepsilon(0,\omega)}\right)_{\exp} \approx \mathrm{Im}\left(\frac{-1}{\varepsilon(q,\omega)}\right)_M = \sum_n \frac{A_n}{E_n^2}\mathrm{Im}\left(\frac{-1}{\varepsilon_M(q,\omega,\gamma_n,E_n)}\right) \tag{13}$$

Note that the fitting procedure does not change in the case of the Mermin model, while we don't need to choose the type of dispersion relation, extension to arbitrary momentum occurs automatically. Fitting coefficients for the ELF of the valence band and of the inner shells for polyethylene, water and DNA are presented in Tables 1, 2 and 3.

Table 1

The coefficients of the energy loss function of polyethylene (C_2H_4) in the form of oscillator functions, Eq. (5)

Type of shell	E_n	A_n	γ_n
Valence band	23	340	15
K-shell C	305	145	180
Phonon peaks $n^{os}=3$	0.09	2e-5	0.005
	0.182	27e-6	0.005
	0.36	4e-4	0.011

Table 2

The coefficients of the energy loss function of water in the form of oscillator functions, Eq. (5)

Type of shell	E_n	A_n	γ_n
Valence band $n^{os}=3$	22	170.3	14
	34	96.75	19
	47	110.45	32
K-shell O	500	150	400

Table 3

The coefficients of the energy loss function of DNA ($C_{20}H_{27}N_7O_{13}P_2$) in the form of oscillator functions, Eq. (5)

Type of shell	E_n	A_n	γ_n
Valence band $n^{os}=7$	4.8	0.07	0.5
	6.8	0.15	1.2
	13.9	5.18	5.5
	18.5	20.8	6.8
	22.2	133	11
	26.2	62	8.8
	34.7	181	21
L-shell P	112	110	140
K-shell C	220	180	200
K-shell N	300	170	270
K-shell O	510	145	365
K-shell P	1850	25	1350

In this work we obtained exact expressions for each Mermin-type oscillator and found the analytical form for Mermin-type ELF. Give them here (we use here atomic units).

The Lindhard dielectric function [13] given as

$$\varepsilon_L(q,\omega)=\varepsilon_{RPA}(q,\omega)\big|_{T=0}=1-\frac{8\pi}{q^2}\int\frac{d^3k}{(2\pi)^3}\frac{f_k-f_{k-q}}{\varepsilon_k-\varepsilon_{k-q}-(\omega+i0)} \tag{14}$$

here integration over the magnitude of the momentum is from zero to Fermi level $k_F=(3\pi^2 n_e)^{\frac{1}{3}}$, n_e is the electron density which can be found from external parameter $E^2=\frac{4\pi n_e}{m}$, f_k is the Fermi distribution function.

For the case of complex frequencies Lindhard function can be represented as:

$$\varepsilon_L(q,\omega+i\gamma)=1+\frac{2}{\pi q^3}\left(\chi_1(q,\omega,\gamma)+i\chi_2(q,\omega,\gamma)\right) \tag{15}$$

$$\chi_1(q,\omega,\gamma)=\frac{1}{2}\int_0^\infty f_k k dk\left[\log\left(\frac{(kq+q^2/2+\omega)^2+\gamma^2}{(kq-q^2/2-\omega)^2+\gamma^2}\right)+\log\left(\frac{(kq+q^2/2-\omega)^2+\gamma^2}{(kq-q^2/2+\omega)^2+\gamma^2}\right)\right] \tag{16}$$

$$\begin{aligned}\chi_2(q,\omega,\gamma)=\int_0^\infty f_k k dk\Bigg[&\arctan\left(\frac{q^2/2+\omega+kq}{\gamma}\right)-\arctan\left(\frac{q^2/2+\omega-kq}{\gamma}\right)-\\&-\arctan\left(\frac{q^2/2-\omega+kq}{\gamma}\right)+\arctan\left(\frac{q^2/2-\omega-kq}{\gamma}\right)\Bigg]\end{aligned} \tag{17}$$

All integrals above easily taken in elementary functions. Take into account that zero-frequency Lindhard function degenerates to Tomas-Fermi screening function $\varepsilon_L(q,0)=1+\frac{q_{TF}^2}{q^2}$, $q_{TF}=4\left(\frac{3n_e}{\pi}\right)^{1/3}$ and give the exact expression for the Mermin ELF

$$\mathrm{Im}\left(\frac{-1}{\varepsilon_M(q,\omega)}\right)=\frac{\frac{\pi q^3}{2}\omega(\gamma\chi_1+\omega\chi_2)-\gamma\omega\frac{q^2}{q_{TF}^2(\chi_1^2+\chi_2^2)}}{\left(\omega\left(\chi_1+\frac{\pi q^3}{2}\right)-\gamma\chi_2\left(1+\frac{q^2}{q_{TF}^2}\right)\right)^2+\left(\omega\chi_2+\gamma\chi_1\left(1+\frac{q^2}{q_{TF}^2}\right)\right)^2} \tag{18}$$

So Mermin-type oscillator term is obtained by replacing $E\to E_n,\quad \gamma\to\gamma_n$.

2.5 Comparisons between approaches

Using the coefficients from Tables 1-3, the inelastic mean free paths and energy losses for scattering electrons are calculated using the equations (2) and (3). Fig. 1 presents the comparison of calculated inelastic mean free paths for all types of models for water with those from the work of Abril et al. [14]. A very good agreement of presented calculations (especially free-electron approximation with plasmon integration limit) confirms the validity of estimated cross section of the electron scattering.

Fig. 2 and 3 present the same comparison for Mermin model and free-electron approximation with work of Abril et al. [14] and also experimental calculations of the inelastic mean free paths from the work of Tanuma et al. [15] and of the energy loss from the work [16].

Based on the presented results, the most suitable model was selected the free-electron approximation. It is in good agreement with experimental data and other calculations, and also requires the least computational cost, which is of great importance when modelling large complex systems.

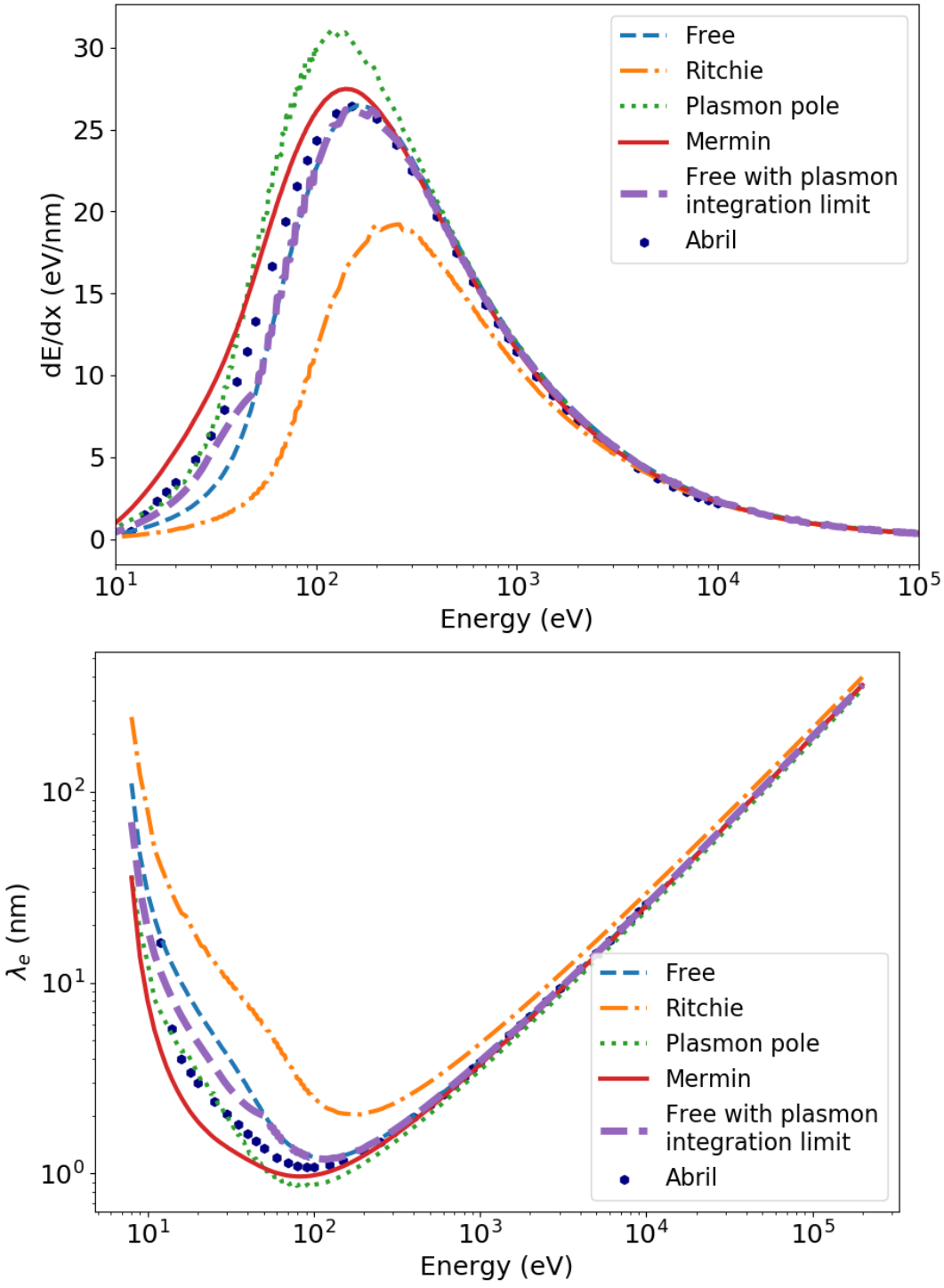

Fig. 1. The IMFPs (a) and energy losses (b) for water. Blue dots correspond to [14]

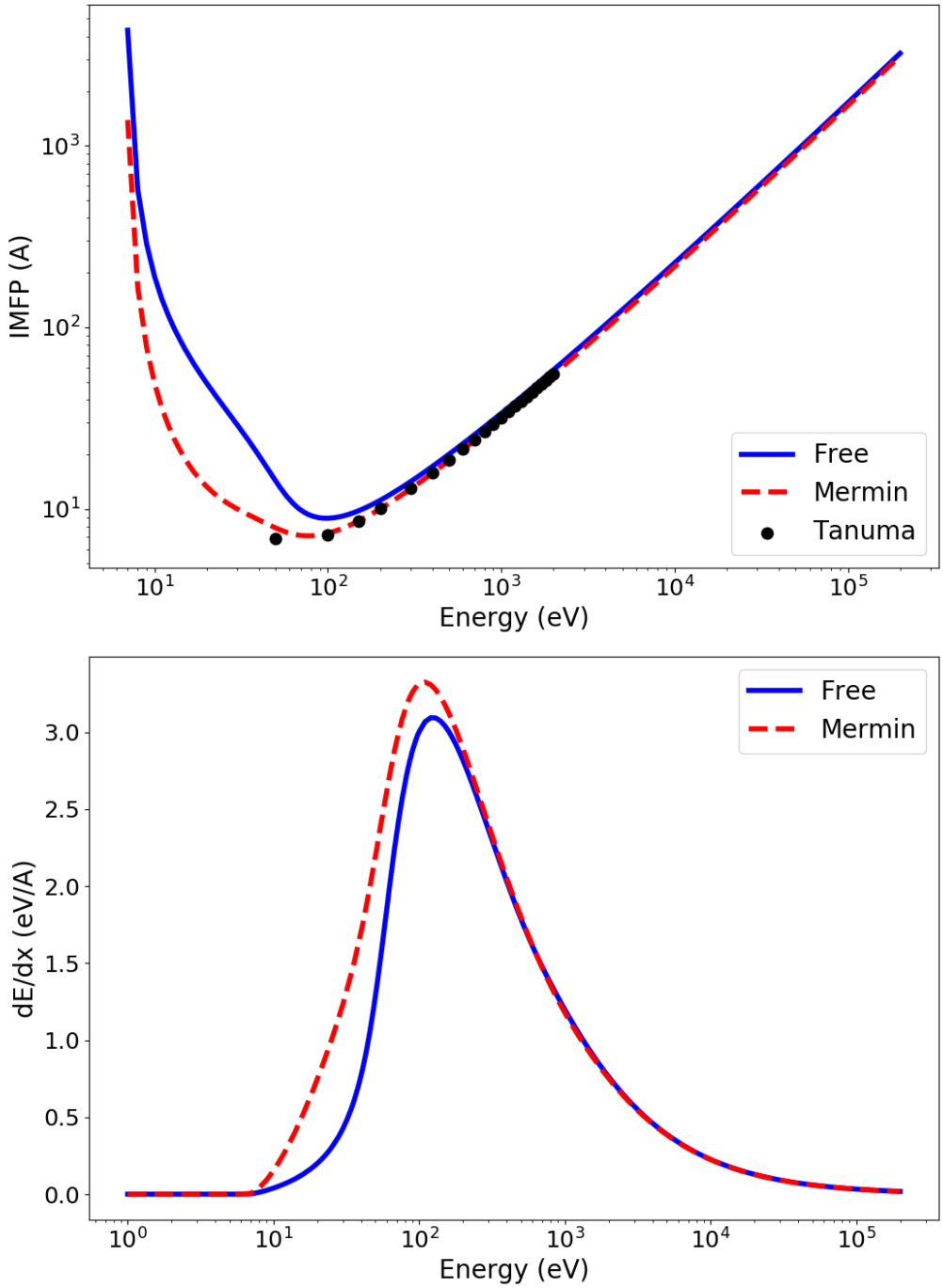

Fig. 2. The IMFPs (a) and energy losses (b) for polyethylene compared with data from Tanuma et al. [15] (black circles)

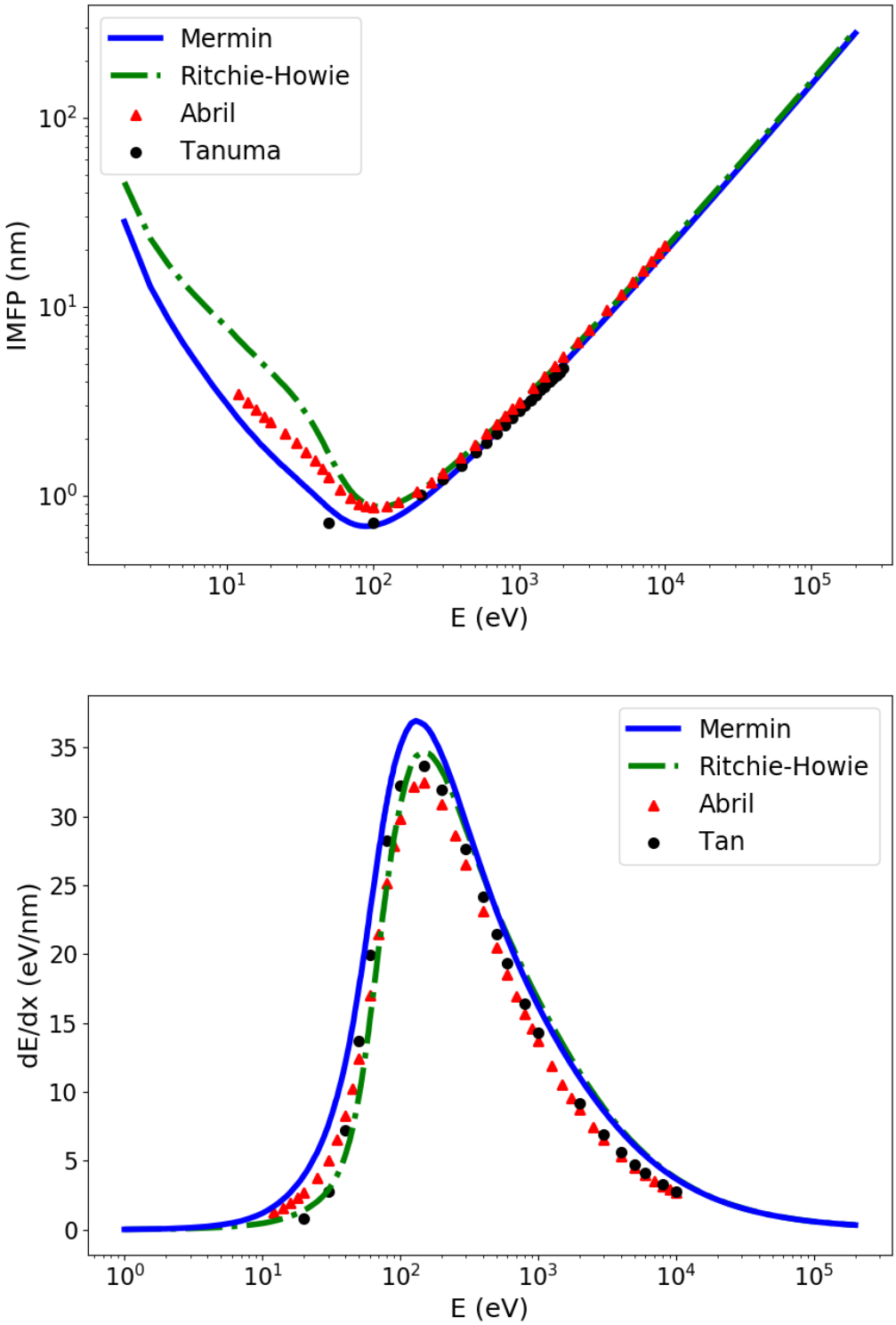

Fig. 3. The IMFPs (a) and energy losses (b) for DNA compared with data from Tanuma et al. [15], Abril et al. [14] and Tan et al. [16]. Here «Ritchie-Howie» label means free-electron approxiamtion.

3 Monte Carlo modelling of SHI track in polyethylene

3.1 MC code TREKIS description

CDF formalism allows to take into account, on the one hand, pair scatterings of a charged projectile on particles of the scattering ensemble, and on the other hand, the collective response of the scattering system and correlations between particles in the system. Developed by Ruslan Rymzhanov and Nikita Medvedev Monte Carlo code TREKIS [2] uses these advantages of CDF formalism. TREKIS based on event-by-event simulations and now includes such processes: propagation of an SHI and the corresponding ionization of target atoms, scattering of primary electrons produced by a SHU, kinetics of all generations of electrons and holes arisen during electron subsystem relaxation, Auger decays of deep shell holes.

Frist TREKIS simulates the initial ionizations of target atoms by an ion creating the 1st generation of electrons in the cylindrical layer with the periodic boundary conditions along the direction of the ion penetration. Atomic electrons are assumed to be independent particles and interaction with SHI is instantaneous. The energy transfer to electrons is calculated using cross section (1), and the direction of propagation of an electron is chosen in accordance with energy and momentum conservation.

The probability of scattering of created free electrons is simulated using the Poisson distribution of the free paths with mean free path calculated by (2). Energy transfer and scattering angle are calculated from cross section. The new electron generation produced in the collision receives energy difference between energy transfer and threshold energy for a given shell. Propagations of the next generations are modeled in the same manner as of the 1st generation.

Inelastic scattering produces also holes in different atomic shells. The holes in inner shells are relaxing via Auger decays and all are popping up into the valence band. The inner shells participating in the Auger decays are chose randomly.

The MC procedure is iterated about 1000 times to obtain realistic statistics. Radial distributions of electrons, phonons and holes and their energy densities in a SHI track are written to the files. Next these distributions are used for initial conditions in further molecular dynamics modelling of lattice transformations and phase transitions.

3.2 Results for polyethylene

For modelling we used an Pb ion with energy of 850 MeV giving the energy loss 1375.61 eV/A. Calculated energy loss is presented in Fig. 4 and compared with results of the SRIM code. Good enough agreement confirms an applicability of chosen model and fitting coefficients. The positions of the Bragg peck are close to each other but not the same. It is expected in relation with various models.

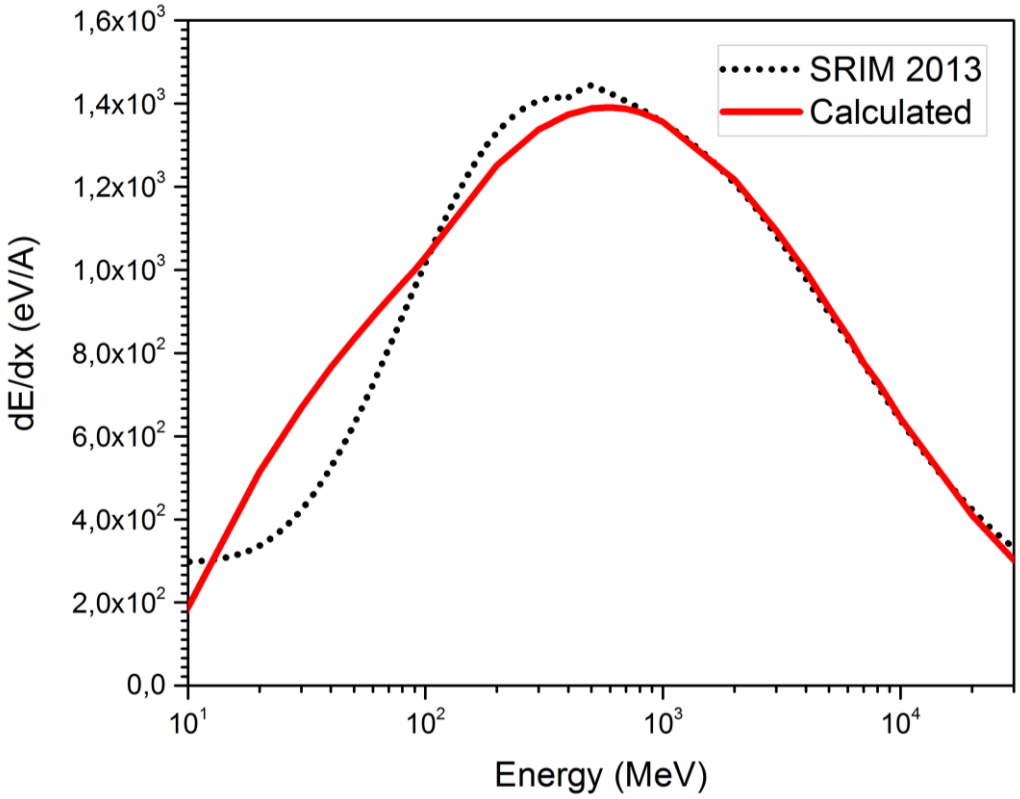

Fig. 4. The calculated energy losses of Pb ion in polyethylene ans function of the ion energy compared to the SRIM data

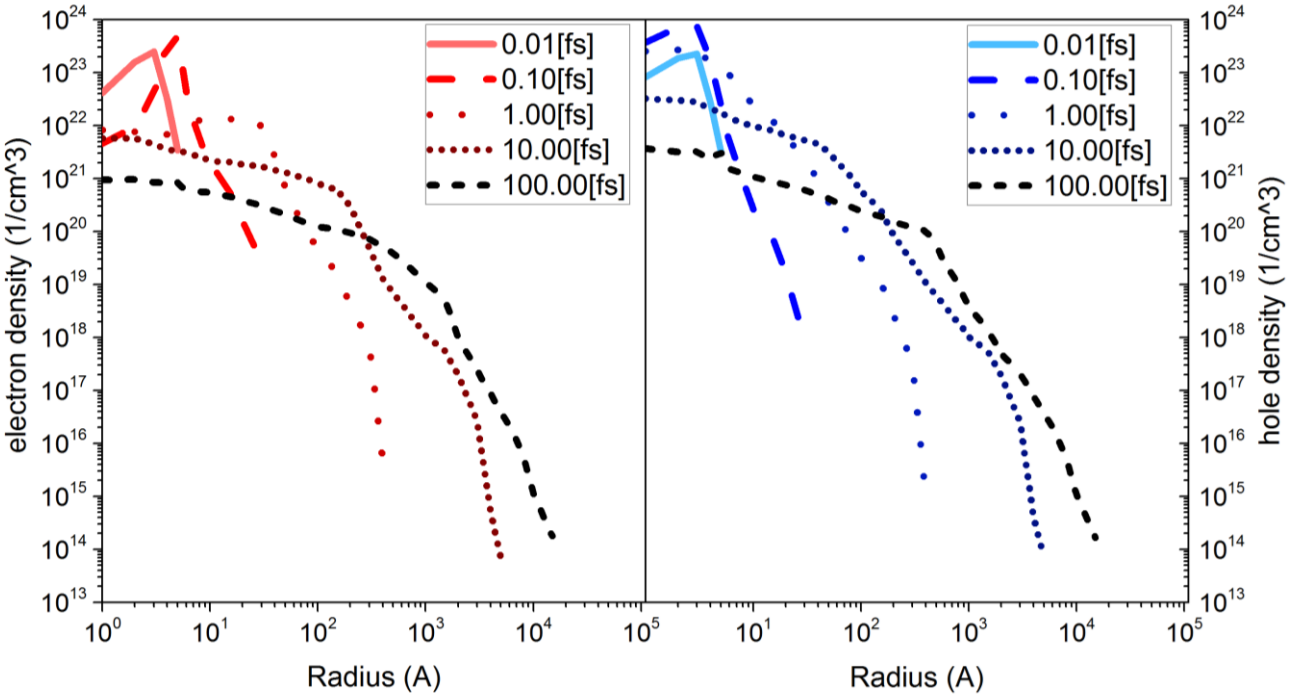

Fig. 5. The calculated electron (a) and hole (b) radial density distributions around the trajectory of Pb ion with energy 850 MeV at different times

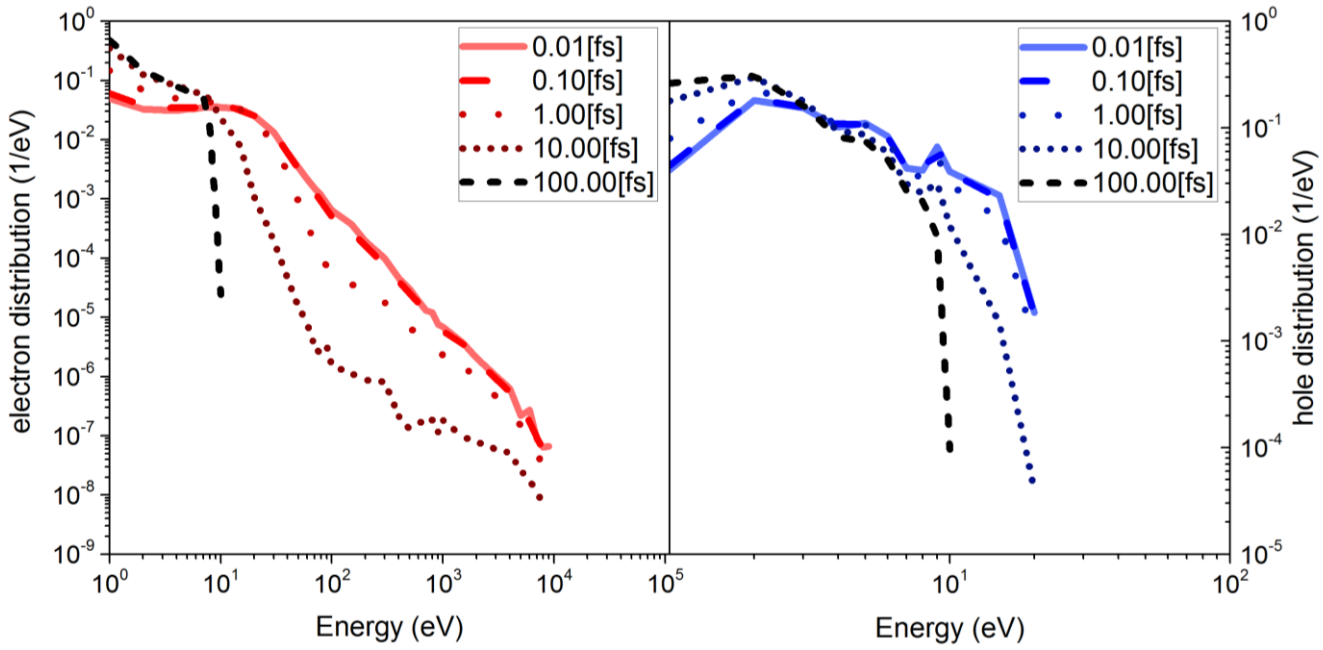

Fig. 6. The calculated electron (a) and hole (b) spectral distributions around the trajectory of Pb ion with energy 850 MeV at different times

Fig. 5 presents the temporal dependencies of the radial density distributions of electrons (a) and holes (a) in polyethylene. Electron and hole energy spectra demonstrated in Fig. 6 it may be noted that electrons and holes are fast spreading from the track core, but first of all electrons bring a considerable part of deposited energy.

4 Molecular Dynamics modelling of track formation

4.1 Modelling parameters

As a system for molecular dynamics modelling was chosen amorphous polyethylene cubic box with 1000 polyethylene chains (see Fig. 7) with 1000 monomers per chain. First the box was minimized using LAMMPS code with such MD parameters: periodic boundary conditions, DREIDING coarse-grained force field [17], which includes valence and Wan-der-Vaals interactions, and six equilibration steps: 1) Langevin dynamics at the temperature 500 K, 2) Nose-Hoover dynamics with NPT thermostat at the temperature 500 K, NPT 3) cooling from 500 K to 100 K, 4) relaxation at 100 K, 5) heating from 100 K to 300 K, and finally, 6) relaxation at 300 K.

After minimization energy transferred to the lattice was emitted to the box as initial condition for further MD modelling. Due to periodic boundary conditions we assumed that the cell is in contact with another cells and we fixed X and Y boundaries at the temperature 300 K and tracked the evolution of the system for 100 ps.

To assess the formation of the track, we used two criteria: displacement magnitude of particles in the center of cell and radial density distribution. Results are shown in Fig. 8 and 9.

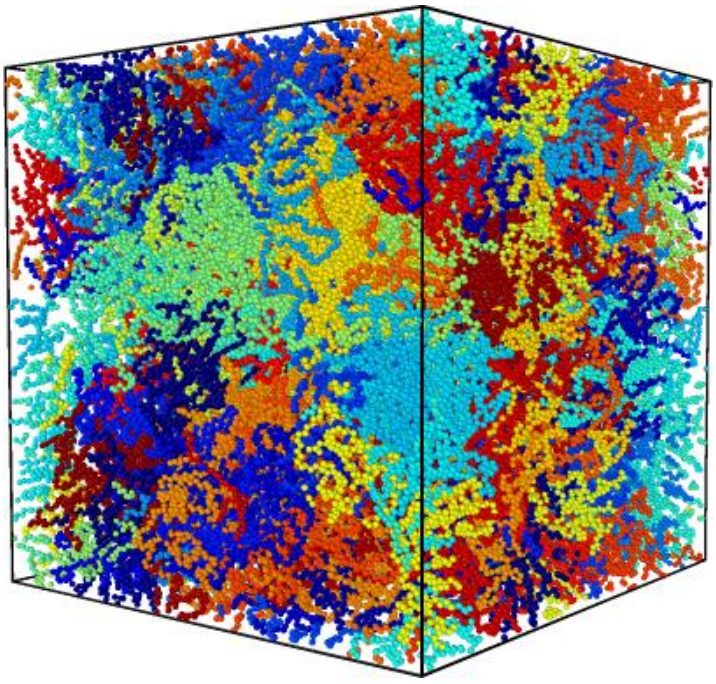

Fig. 7. Amorphous polyethylene cell with 1000 chains with 1000 monomers per cell. Each monomer is coarse grained particle, fromed from two hydrogen atoms and one carbon atom. Cell was prepared with random walking algorithm

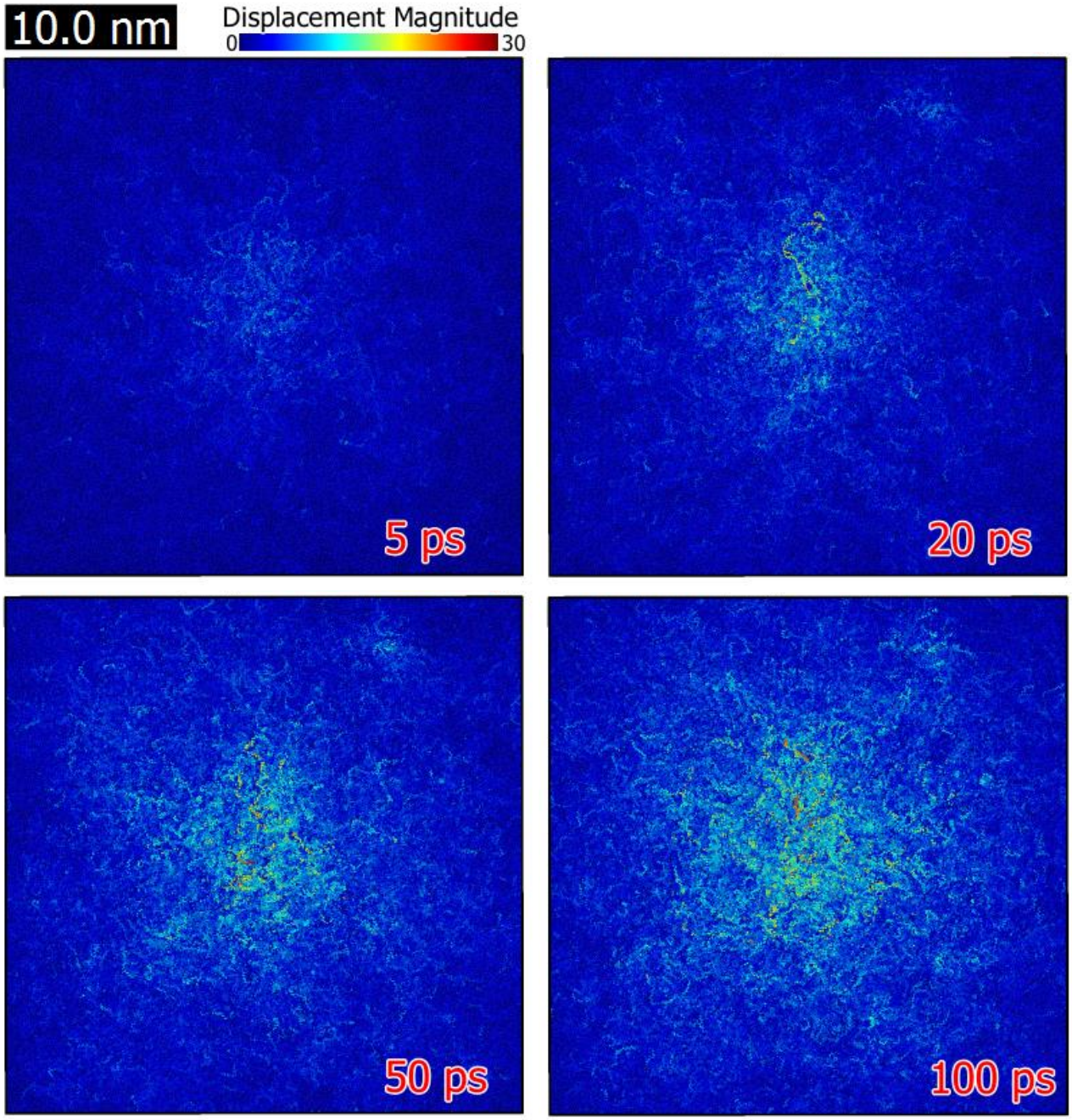

Fig. 8. Displacment of particles (view from above) at different times after SHI passage

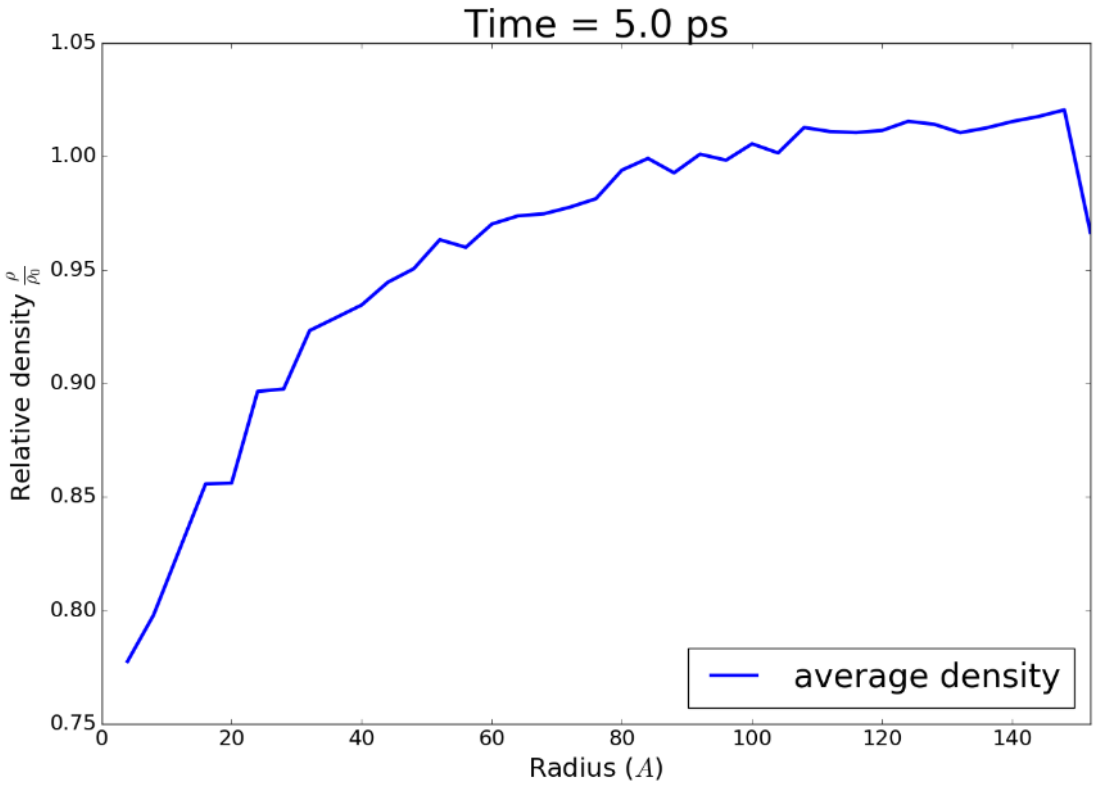
Time = 5.0 ps
Relative density $\frac{\rho}{\rho_0}$
Radius (A)
average density
1.05
1.00
0.95
0.90
0.85
0.80
0.75
0
20
40
60
80
100
120
140

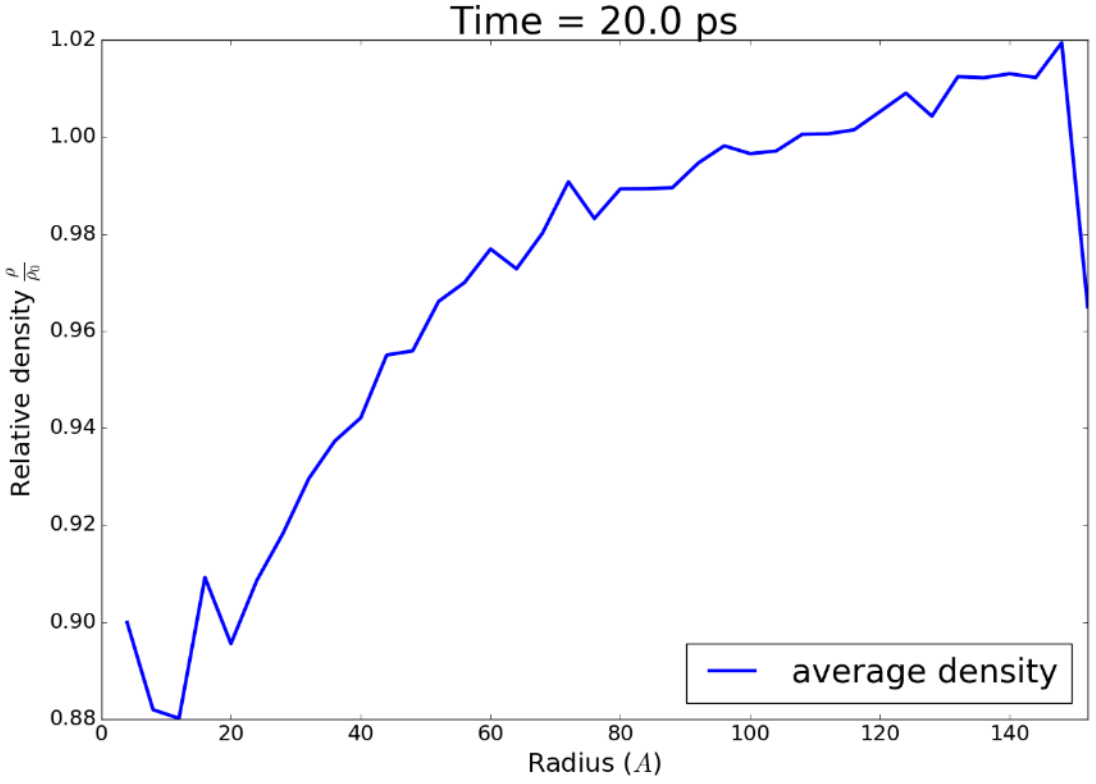
Time = 20.0 ps
Relative density $\frac{\rho}{\rho_0}$
Radius (A)
average density
1.02
1.00
0.98
0.96
0.94
0.92
0.90
0.88
0
20
40
60
80
100
120
140

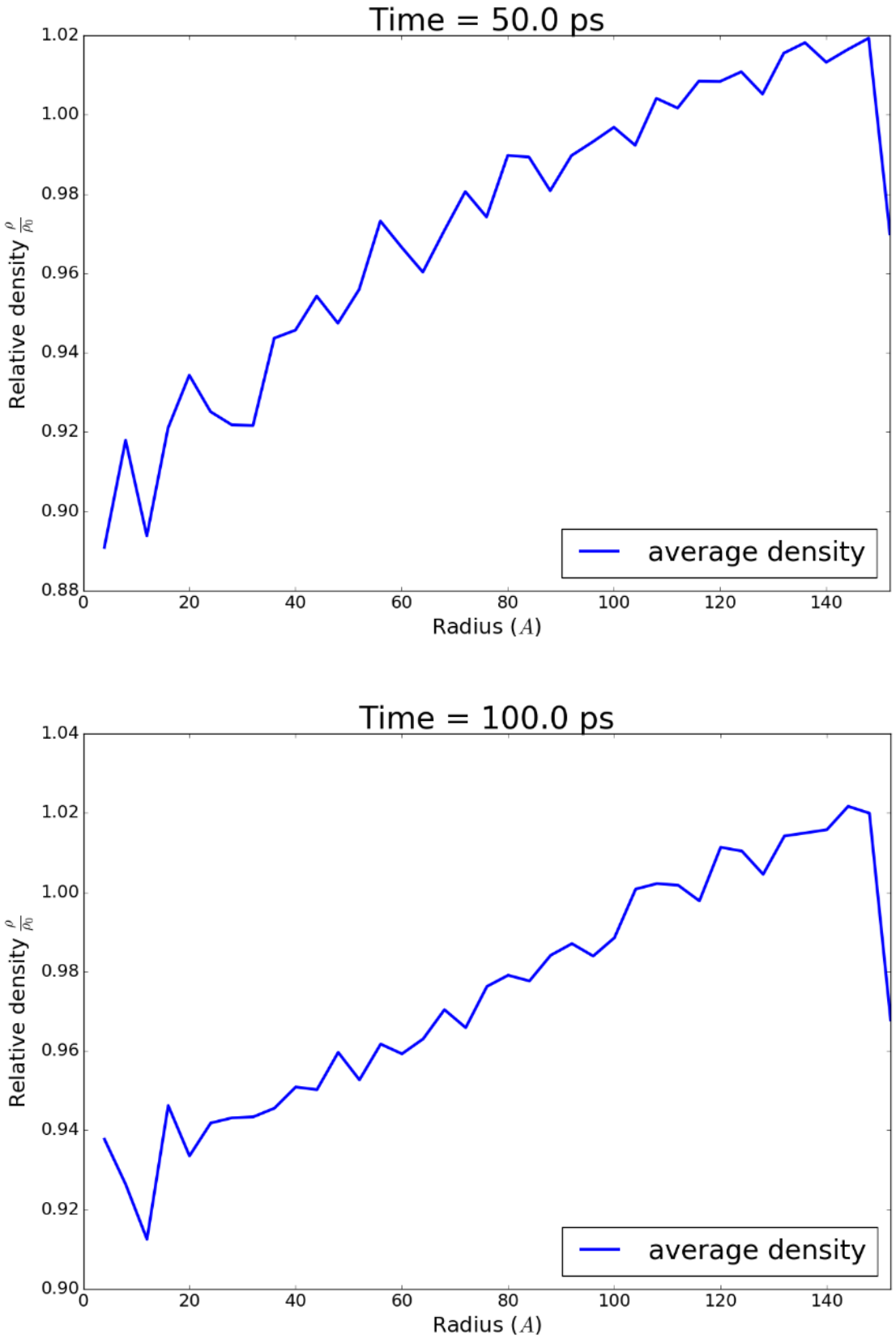

Fig. 9. Radial density distribution at different times after SHI passage

4.2 Discussion

According to Fig. 8 and 9 and our calculations after 5 ps begins relaxation of the cell, the density is slowly leveling to average, track becomes hidden. Note that density increase near the boundary follows from periodic boundary conditions, particles does not leave the box, so it is artefact of modelling. Effective radius of the track is about 60 or 80 angstroms. We expected a density drop of about 20-30 percent, but in this modelling it is not observed. We suppose that it is related with a bad choice of force field, modelling with full-atoms force fields is required. Anyway, even with a coarse-grained force field modelling predicts track formation in amorphous polyethylene. It is important result in light of the further research of more complicated biopolymers such DNA or nucleotides.

5 Conclusion

In this work we found exact form of Mermin energy loss function and also implemented Mermin-type oscillator terms within TREKIS code. We showed that, on the one hand, Mermin model works well in cause of biomolecules, and on the other hand, free-electron approximation also gives good results for biomolecules and requires less computational resources. Next we used free-electron approximation for construction cross sections for MC modelling and calculated Pb ion propagation through polyethylene target. The energy distribution obtained after MC calculation was used as initial condition for molecular dynamics of track formation.

MD results don’t give a clear answer to the question about track formation in amorphous polyethylene, more detailed research is required. We plan to model a SHI track formation using full-atom potentials and search another, more accurate criteria of phase transition in amorphous solids.

We will also continue to work on modelling all stages of DNA excitation and relaxation after the passage of an SHI.

References

1. Komarov F.F. Defect and track formation in solids irradiated by superhigh-energy ions // Physics-Uspekhi. 2003. Vol. 46, № 12. P. 1253–1282.
2. Medvedev N.A., Rymzhanov R.A., Volkov A.E. Time-resolved electron kinetics in swift heavy ion irradiated solids // J. Phys. D. Appl. Phys. 2015. Vol. 48, № 35. P. 355303.
3. Baranov A.A. et al. Effect of interaction of atomic electrons on ionization of an insulator in swift heavy ion tracks // Nucl. Instruments Methods Phys. Res. Sect. B Beam Interact. with Mater. Atoms. North-Holland, 2012. Vol. 286. P. 51–55.
4. Van Hove L. Correlations in Space and Time and Born Approximation Scattering in Systems of Interacting Particles // Phys. Rev. American Physical Society, 1954. Vol. 95, № 1. P. 249–262.
5. Ritchie R.H., Howie A. Electron excitation and the optical potential in electron microscopy // Philos. Mag. Taylor & Francis Group , 1977. Vol. 36, № 2. P. 463–481.
6. Kubo R. The fluctuation-dissipation theorem // Reports Prog. Phys. 1966. Vol. 29, № 1. P. 255–284.
7. BETZ H.-D. Charge States and Charge-Changing Cross Sections of Fast Heavy Ions Penetrating Through Gaseous and Solid Media // Rev. Mod. Phys. American Physical Society, 1972. Vol. 44, № 3. P. 465–539.
8. Akkerman A. et al. Inelastic electron interactions in the energy range 50 eV to 10 keV in insulators: Alkali halides and metal oxides // Phys. Status Solidi Basic Res. 1996. Vol. 198, № 2. P. 769–784.
9. Palik E.D. Handbook of optical constants of solids // Unknown Journal. 1998. Vol. 1, № v. 3. 900 p.
10. Henke B.L., Gullikson E.M., Davis J.C. X-Ray Interactions: Photoabsorption, Scattering, Transmission, and Reflection at E = 50-30,000 eV, Z = 1-92 // At. Data Nucl. Data Tables. Academic Press, 1993. Vol. 54, № 2. P. 181–342.

11. Ding Z.-J., Shimizu R. Inelastic collisions of kV electrons in solids // Surf. Sci. North-Holland, 1989. Vol. 222, № 2–3. P. 313–331.
12. Mermin N.D. Lindhard dielectric function in the relaxation-time approximation // Phys. Rev. B. 1970. Vol. 1, № 5. P. 2362–2363.
13. Ashcroft N.W., Mermin N.D. Физика твердого тела. Mir, 1979. № т. 1.
14. Garcia-molina R., Abril I. Inelastic scattering and energy loss of swift electron beams in biologically relevant materials. 2016. № July 2015.
15. Tanuma S., Powell C.J. Electron Inelastic Mean Free Paths. 5. Data for 14 organic-compunds over the 50-2000 eV range // Surf. Interface Anal. 1994. Vol. 21, № September 1993. P. 165–176.
16. Tan Z. et al. Electron inelastic interactions in bioorganic compounds in the energy range of 20-10000 eV // Appl. Phys. A Mater. Sci. Process. 2005. Vol. 81, № 4. P. 779–786.
17. Mayo S.L., Olafson B.D., Goddard W.A. DREIDING: A generic force field for molecular simulations // J. Phys. Chem. 1990. Vol. 94, № 26. P. 8897–8909.